Digest Journal of Nanomaterials and Biostructures Vol. 18, No. 4, October-December 2023, p.1159-1167

Nickel oxide doping impact on the NO_2 sensing properties of nanostructured zinc oxide deposited by spray pyrolysis

M. J. Dathan[a], B. F. Hassan[a], Q. A. Abduljabbarb[b], J. M. Rzaij[c,*]
[a]*General Directorate of Education in Salah al-Din, Salah al-Din, Iraq*
[b]*Minstry of Education, Salah AL-din*
[c]*Department of Physics, College of Science, University Of Anbar, Ramadi, Iraq*

In this study, zinc oxide was doped with varying Nickel oxide nanostructured thin film concentrations using spray pyrolysis at 400 °C. At low Ni content, the ZnO phase exhibited polycrystalline structures, whereas a high Ni concentration resulted in the development of an additional NiO phase. The morphological analysis indicates the presence of nano-spherical structures at lower Ni concentrations, with nanoflakes embedded at varying orientations. The density of the nanoflakes structure was observed to increase as the Ni content was increased, enhancing the surface-to-volume ratio, which has potential applications in gas sensing. The highest sensitivity was detected for the sample doped with the highest Ni content, which can be attributed to its superior effective surface area. The optimal sensitivity was 45.26% at 200 °C.

(Received June 21, 2023; Accepted September 25, 2023)

Keywords: ZnO, Nickel oxide, Gas sensor, Spray pyrolysis, NO_2

1. Introduction

Hazardous gases encompass gaseous substances with toxic, flammable, or environmentally harmful properties. In order to guarantee occupational safety, it is imperative to detect any potential gas leakage at the lowest concentrations feasible [1]. The capability to observe the environment from damaging gases using small and low-cost devices is a subject of countless attention in numerous studies. Metal oxide-based gas sensors, which are the head of this study, have good sensitivity, low cost, and high stability gas substances and are easy to measure using simple circuits [2,3]. Recently, metal oxide has been rewarded with more special treatment due to its diverse function and promising application in various fields [4,5].

The optimization of gas sensor performance necessitates a focus on the size and shape of nanostructures, as this impacts surface area and the number of atoms on the sensor surface [6]. Consequently, the primary objective is maintaining control of the size and shape of particles at the nanoscale to enhance gas sensor efficiency [7]. A variability of nanostructures has design comprised of different types of zero-dimension, one-dimension, and two-dimension structures [8]. The spray pyrolysis technique is a promising method for simply depositing large coating areas of numerous thin films such as metal oxides [2,9,10].

The process of oxygen absorption by metal oxide from the surrounding environment and its subsequent transformation into ion species through the capture of electrons from the material's surface leads to the formation of a surface depletion layer. The interaction of these ions with gas molecules causes variation in the depletion layer causing a fluctuation in gas resistance outstanding to the return or removed additional electrons [11]. These changes in the resistance can be converted as a signal to be detected in a gas sensor electronic device [12]. Upon exposure to an oxidizing gas, an n-type semiconductor undergoes catalytic reduction with the adsorbed oxygen species, resulting in the release of electrons back into the conduction band of the semiconductor surface [13].

*Corresponding author: sc.jam72al@uoanbar.edu.iq
https://doi.org/10.15251/DJNB.2023.184.1159

Due to a reduction in charge carrier concentration or thickening of the depletion layer which in turn reduces charge carrier mobility, this process reduces the sample conductivity of n-type semiconductors [14]. This study investigates the structural characteristics, surface morphology, and nitrogen dioxide detection capabilities at low concentrations of NiO-doped ZnO films developed via the chemical spray pyrolysis technique. The present study aimed to investigate the impact of varying concentrations of nickel oxide doping on the gas-sensing properties of the synthesized films at various operating temperatures when exposed to different NO2 concentrations.

2. Experimental

2.1. Materials and thin films characterization

Nickel chloride ($NiCl_2$) and Zinc chloride ($ZnCl_2$) of 99.9% purity are provided by Sigma-Aldrich company to synthesize thin films gas sensors. The structural properties of the deposited $(ZnO)_{1-x}(NiO_2)_x$ thin films at varying NiO molar ratios (x=0.01, 0.02, 0.03, and 0.04) were determined using the X-ray diffraction (XRD) technique, specifically the SHIMADZU XRD-6000. Meanwhile, the surface morphology of the thin films was examined using scanning electron microscopy (SEM), specifically the Jeol JSM 6335F. The gas sensing analysis was investigated within a glass chamber placed on a hot plate with a controlled temperature. The controlled electrical valve allows the entry of the gas-air mixture into the chamber, measured by a flow meter. The temporal evolution of the sample's resistance was investigated under the gas presence (Gas ON) and absence conditions (Gas OFF), utilizing a multimeter that was interfaced with a computer.

2.2. Samples preparation

Thin films of NiO-doped ZnO were deposited on glass substrates at 400 °C using the spray pyrolysis technique. The deposition was carried out from an aqueous mixture of zinc chloride and nickel chloride with varying NiO molar ratios, at a concentration of 0.1 M. The pH of the solution was adjusted at pH=5 by adding a few drops of hydrochloric acid. The solution was sprayed by a fine atomizer installed 30 cm above the substrate. The experimental protocol involved the implementation of a spray duration of 5 seconds and a stop duration of 10 seconds, with a spray rate of 2 ml/min, utilizing compressed air at a pressure of 5 bar. After the 20 ml spray, the sample is finally allowed to remain on the substrate for 20 minutes at the same temperature before being removed after cooling. Thermal evaporation under a high vacuum Edward coater was used to deposit appropriate aluminum electrodes on the sample surface, as shown in Fig. 1.

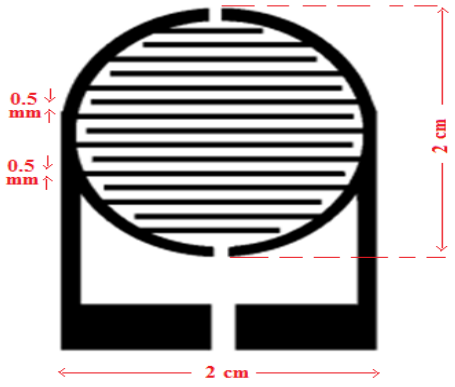

Fig. 1. Gas sensor electrode dimensions.

3. Results and Discussions

The x-ray diffraction spectra of the ZnO:NiO thin films on glass substrates at varying NiO atomic ratios at a temperature of 400 °C are depicted in Fig. 2. The investigation of the structural properties indicated that the deposited films exhibited a polycrystalline nature. Furthermore, it was observed that the ZnO phase dominated when the NiO dopant ratio was low (x=0.01). This observation suggests that the Ni atoms were incorporated into the host lattice without substantially altering its structure. Four peaks appeared at diffraction angles 31.8002°, 34.3056°, 36.2126°, and 47.5427° corresponding to the (110), (002), (101), and (102) plains, respectively, for hexagonal ZnO structure. An increase in the NiO ratio was caused by the advent of the NiO phase addition to the ZnO one, and this phase crystallinity was enhanced while the ZnO phase reduced with increasing the NiO content. The structural parameters of the prepared films are shown in Table 1.

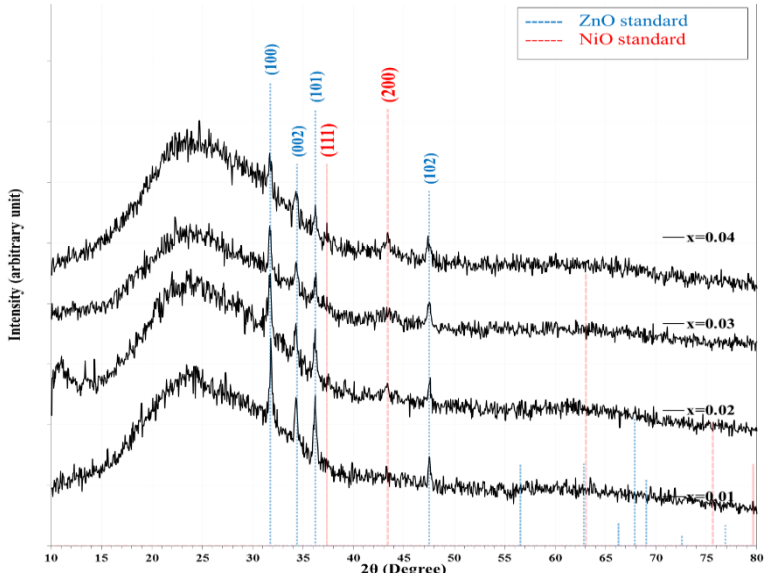

Fig. 2. XRD diagram of ZnO:NiO thin films at different x-molar ratios.

Table 1. XRD characteristics of ZnO:NiO thin films at various NiO (x-contents).

x-contents	2θ (Deg.)	FWHM (Deg.)	d_{hkl} (Å)	C.S (nm)	Phase	hkl
0.01	31.8002	0.2992	2.8117	27.6	Hex. ZnO	(110)
	34.3056	0.2991	2.6119	27.8	Hex. ZnO	(002)
	36.2126	0.4114	2.4786	20.3	Hex. ZnO	(101)
	47.5427	0.4113	1.9110	21.1	Hex. ZnO	(102)
0.02	31.7628	0.4113	2.8149	20.1	Hex. ZnO	(110)
	34.3056	0.4113	2.6119	20.2	Hex. ZnO	(002)
	36.1752	0.4114	2.4811	20.3	Hex. ZnO	(101)
	43.3921	0.5983	2.0837	14.3	Cubic NiO	(200)
	47.6175	0.3365	1.9082	25.8	Hex. ZnO	(102)
0.03	31.6880	0.4113	2.8214	20.1	Hex. ZnO	(110)
	34.3056	0.4861	2.6119	17.1	Hex. ZnO	(002)
	36.2874	0.3740	2.4737	22.4	Hex. ZnO	(101)
	43.4669	1.0844	2.0803	7.9	Cubic NiO	(200)
	47.5053	0.5609	1.9124	15.5	Hex. ZnO	(102)
0.04	31.6880	0.4861	2.8214	17.0	Hex. ZnO	(110)
	34.3429	0.5983	2.6091	13.9	Hex. ZnO	(002)
	36.2500	0.4488	2.4761	18.6	Hex. ZnO	(101)
	37.4092	0.6730	2.4020	12.5	Cubic NiO	(111)
	43.3921	0.6356	2.0837	13.5	Cubic NiO	(200)
	47.3932	0.5235	1.9167	16.6	Hex. ZnO	(102)

The scanning electron microscope images of ZnO:NiO thin films at different NiO concentrations are illustrated in Fig. 3. This illustration shows an extended surface with attached 40 nm-diameter nanoparticles. Additionally, the deposited films had an average diameter of 200 nm and a 40 to 50 nm thickness, growing in a flake-like structure into the bulk surface, increasing the surface area of the sample. Increasing the NiO concentration causes to increase in the nanoflake numbers in the unit area, till it becomes of high density and intertwined with each other at the highest NiO contents. These nanoflakes belong to the structure of nickel oxide, as many studies have shown the possibility of NiO deposition in the form of nanoflakes. The surface characteristics of the gas sensors and the shape of the nanostructure are influential factors in improving the properties of the prepared sensors, as they display a large surface-to-volume ratio and thus contribute to enhancing the sensor properties by increasing the number of gas molecules interacting with the surface of the sensor [15,16].

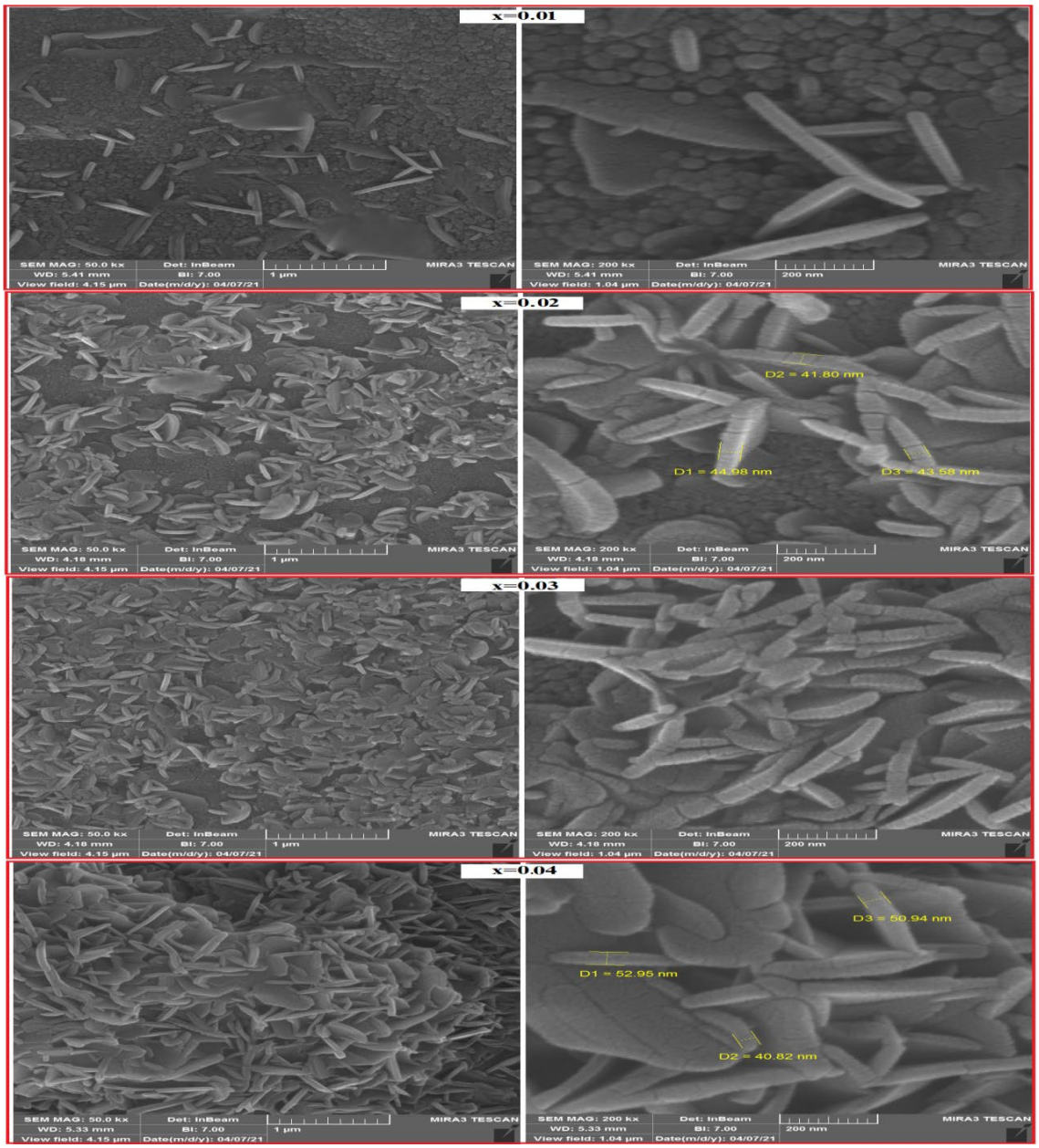

Fig. 3. SEM micrographs of ZnO: NiO nanoflakes thin film at different NiO concentrations.

Fig. 4 depicts the temporal evolution of electrical resistance for a ZnO:NiO thin film sensor at varying concentrations of NiO and a constant operating temperature of 200 °C, as illustrated in. The sensor's electrical resistance increases when exposed to NO_2 (green arrow) at a concentration of 50 ppm. Still, it returns to the baseline when the gas is removed (red arrow), demonstrating the prepared thin films' n-type electrical conductivity [17]. The results suggest that the sensitivity was significantly impacted by the NiO doping ratio, which can be attributed to the observed alterations in surface morphology, as confirmed by the SEM analysis. The sample doped with 0.04 NiO exhibited the most significant sensitivity, owing to its larger surface area resulting from the unique nano-flake structure behavior. The gas sensitivity was determined from the relation [18]:

$$S\% = \frac{\mathrm{R_{gas}} - \mathrm{R_{air}}}{\mathrm{R_{air}}} \times 100\%$$

where $\mathrm{R_{air}}$ and $\mathrm{R_{gas}}$ represents the sample resistance when exposed to clean air and the target gas respectively.

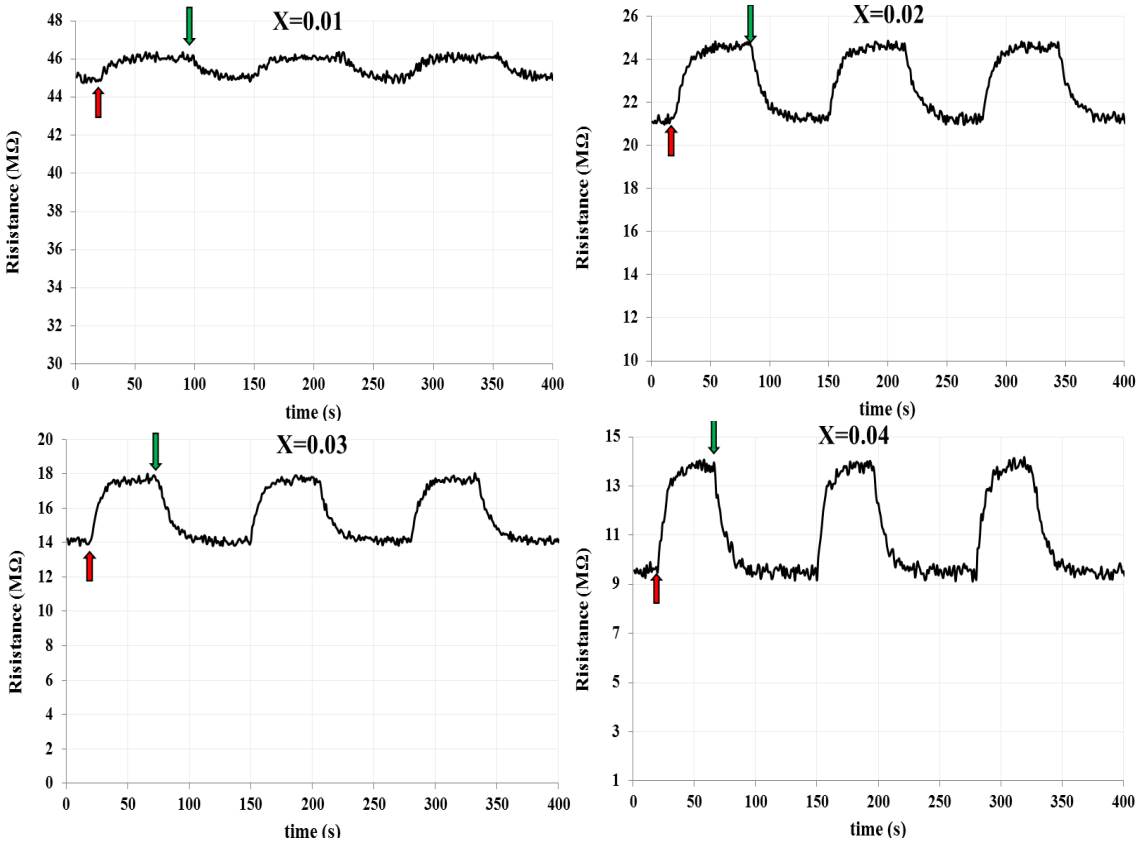

Fig. 4. Electrical resistance variation of the ZnO: NiO nanoflakes gas sensor against 50 ppm NO_2.

The operating temperature is another significant feature of thin film sensors. Fig. 5 depicts the variation of the electrical resistance for the ZnO:NiO thin films at a NiO doping ratio of 0.04 when exposed to 50 ppm NO2 at various operating temperatures ranging from room temperature (27 °C) to 300 °C. The electrical resistance of the sample was more varied at high temperatures. This variation in sensitivity with temperature is due to changes in the dominant reactions between the NO2 gas and the oxygen ions species adsorbing on the sample surface.

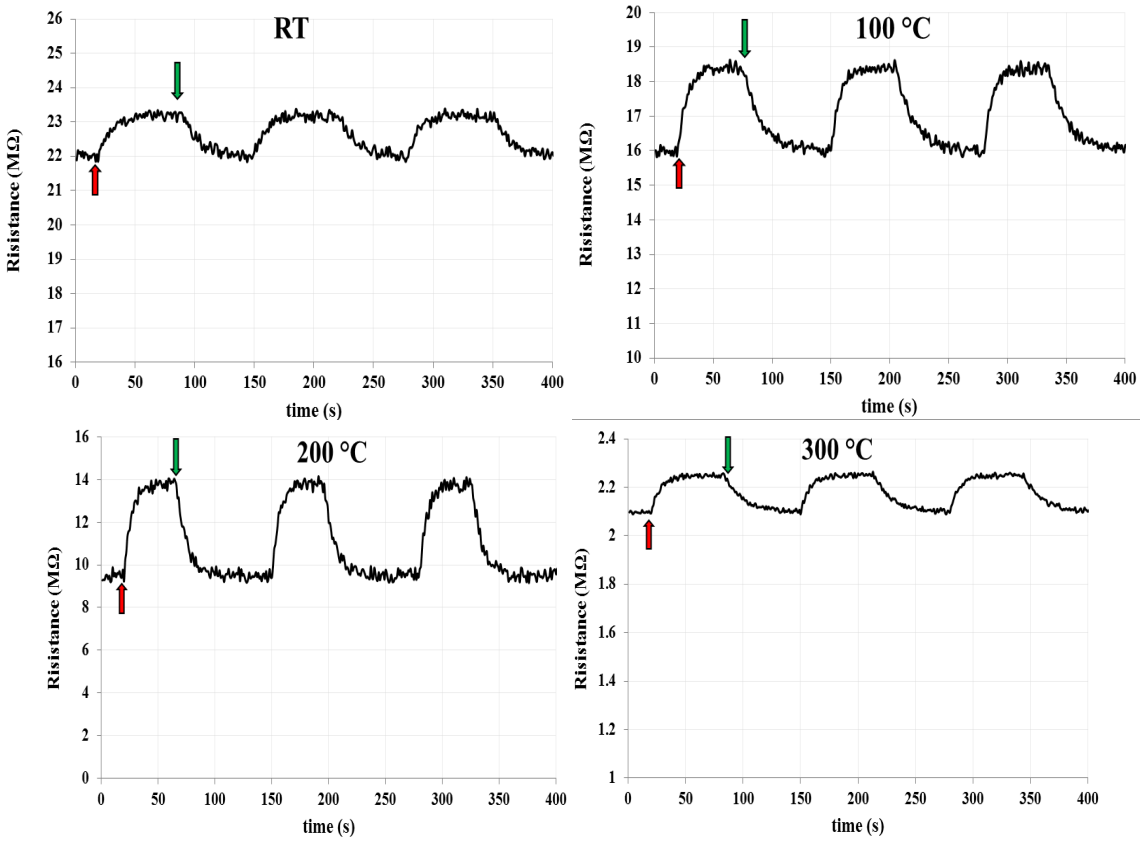

Fig. 5. Electrical resistance at different working temperatures of the $(ZnO)_{1-x}$: $(NiO)_x$ gas sensor against 50 ppm NO_2 at x=0.04.

Fig. 6 illustrates the variation in the sensitivity of the ZnO: NiO thin film gas sensor against 50 ppm NO_2 at varying temperatures of operation. The optimal sensitivity was observed at 200 °C, which may be attributable to the variety of oxygen ion species adsorbing on the active surface and reacting with the target gas. At low temperatures, $O_2^-{}_{ads}$ is the predominant species that attracts electrons from the conduction band of the semiconductor's surface region. The equation that governs the reaction is $O_2^-{}_{ads} + e^- = 2O^-{}_{ads}$ [19], which attracts more electrons from the sample as the temperature rises. At higher temperatures, gas molecules desorb from the sample's surface, reducing the sensitivity [20].

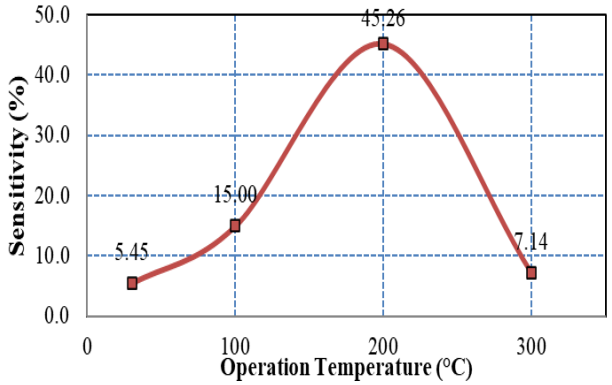

Fig. 6. Variation of the gas sensitivity with the operating temperature against 50 ppm NO_2 gas.

Fig. 7 depicts the variation of ZnO: NiO thin film gas sensor sensitivity against 50 ppm NO_2 at various NiO concentrations. As a result of the variation in surface morphology, increasing the NiO content to 0.04 increased the gas sensitivity [21]. Tables 2 and 3 lists the results of ZnO: NiO nanoflake-based gas sensor analysis at various operating temperatures and NiO concentrations.

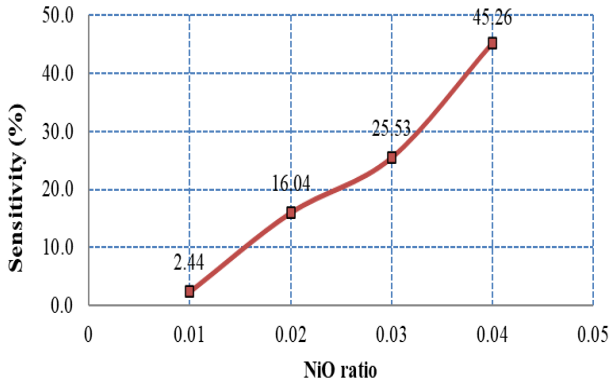

Fig. 7. Variation of the gas sensitivity with NiO ratio at 200 °C operating temperature against 50 ppm NO_2.

The response and recovery time are critical elements that limit the performance requirements of gas sensors. Response/recovery time is defined as the time required to attain a 90% / 10% resistance variation upon exposure/removal of the gas target. The response time of the ZnO: NiO-based sensor at 200 °C operating temperature was shorter than the recovery time of the other samples, as depicted in Table 2. The shorter response/recovery time is potentially due to slower surface reactions, such as desorption and de-ionization, relative to the fast adsorption process [22].

Table 2. The specifications of gas sensors based on ZnO: NiO nanoflakes at various operating temperatures.

Temp. (°C)	Sensitivity %	response time (sec)	recovery time (sec)
30	5.455	30	52
100	15.000	25	45
200	45.263	22	30
300	7.143	28	40

Table 3. The specifications of gas sensors based on ZnO: NiO nanoflakes at different NiO concentrations.

x-ratio	Sensitivity %	response time (sec)	recovery time (sec)
0.01	2.444	32	39
0.02	16.038	28	36
0.03	25.532	25	33
0.04	45.263	22	30

4. Conclusions

The NO_2 gas sensor was fabricated based on ZnO: NiO nanoflakes deposited by spray pyrolysis technique in one step, using doping chloride aqueous solutions at different NiO concentrations. Structural examination shows polycrystalline ZnO structure, and increasing the Ni content caused an additional evident phase of NiO. Microstructure analysis confirmed extended structures composed of nanoflake-like systems orientated randomly. This number of nanoflakes structure per area increased with increasing the Ni content, enhancing the surface features for gas sensing applications. The related sensing properties confirmed this performance since the gas sensitivity improved with increasing the NiO content due to increasing the effective surface area exposed to the target gas.

References

[1] H. Janssen, J. C. Bringmann, B. Emonts, and V. Schroeder, International Journal of Hydrogen Energy 29, 759 (2004); https://doi.org/10.1016/j.ijhydene.2003.08.014

[2] O. S. Shawki and J. M. Rzaij, 1st Diyala International Conference for Pure and Applied Science (ICPAS2021) (AIP Conference Proceedings, 2023), (March), p. 020009; https://doi.org/10.1063/5.0112172

[3] S. Basu, Y. H. Wang, C. Ghanshyam, and P. Kapur, Bulletin of Materials Science 36(4), 521 (2013); https://doi.org/10.1007/s12034-013-0493-9

[4] I. M. Ibrahim, J. M. Rzaij, and A. Ramizy, Digest Journal of Nanomaterials and Biostructures 12(4), 1187 (2017).

[5] A. Kurz and M. A. Aegerter, Thin Solid Films 516, 4513 (2008); https://doi.org/10.1016/j.tsf.2007.05.082

[6] R. Kumar, X. Liu, J. Zhang, and M. Kumar, Nano-Micro Letters 12(146), 1 (2020). https://doi.org/10.1007/s40820-020-00503-4

[7] E. S. Hassan, T. H. Mubarak, K. H. Abass, S. S. Chiad, N. F. Habubi, M. H. Rahid, A. A. Khadayeir, M. O. Dawod, and I. A. Al-Baidhany, Journal of Physics: Conference Series 1234(1), (2019); https://doi.org/10.1088/1742-6596/1234/1/012013

[8] G. Sun, S. Zhang, and Y. Li, International Journal of Photoenergy 2014, 25 (2014); https://doi.org/10.1155/2014/643637

[9] J. M. Rzaij, A. S. Ibraheam, and A. M. Abass, Baghdad Science Journal 18(2), 401 (2021); https://doi.org/10.21123/bsj.2021.18.2.0401

[10] A. Abrutis, G. Valincius, G. Baltrunas, L. Parafionovic, A. Valiuniene, and Z. Saltyte, Thin Solid Films 515, 6817 (2007); https://doi.org/10.1016/j.tsf.2007.02.075

[11] R. Sakthivel and P. M. Shameer, International Journal of Science and Research 4(2), 183 (2015).

[12] J. M. Rzaij and A. Mohsen Abass, Journal of Chemical Reviews 2(2), 114 (2020); https://doi.org/10.33945/SAMI/JCR.2020.2.4

[13] X. Li, X. Li, N. Chen, X. Li, J. Zhang, and J. Yu, Journal of Nanomaterials 2014, 1 (2014); https://doi.org/10.1155/2014/921896

[14] E. Espid and F. Taghipour, Sensors & Actuators: B. Chemical 241, 828 (2017); https://doi.org/10.1016/j.snb.2016.10.129

[15] J. M. Rzaij and N. F. Habubi, Journal of Materials Science: Materials in Electronics 33(15), 11851 (2022); https://doi.org/10.1007/s10854-022-08148-2

[16] J. M. Marei, A. A. Khalefa, Q. A. Abduljabbar, and J. M. Rzaij, Journal of Nano Research 70, 41 (2021); https://doi.org/10.4028/www.scientific.net/JNanoR.70.41

[17] Q. A. Abduljabbar, H. A. Radwan, J. M. Marei, and J. M. Rzaij, Engineering Research Express 4(1), 015028 (2022); https://doi.org/10.1088/2631-8695/ac57fb

[18] M. A. Kadhim, A. A. Ramadhan, and M. O. Salman, Karbala International Journal of Modern Science 6(1), 83 (2020); https://doi.org/10.33640/2405-609X.1403

[19] L. Francioso, A. Forleo, S. Capone, M. Epifani, A. M. Taurino, and P. Siciliano, Sensors and Actuators B 114(2), 646 (2006); https://doi.org/10.1016/j.snb.2005.03.124

[20] Y. F. Sun, S. B. Liu, F. L. Meng, J. Y. Liu, Z. Jin, L. T. Kong, and J. H. Liu, Sensors 12(3), 2610 (2012); https://doi.org/10.3390/s120302610

[21] M. A. Kadhim, A. A. Ramadhan, and M. O. S. Al-Gburi, Karbala International Journal of Modern Science 7(1), (2021); https://doi.org/10.33640/2405-609X.2486

[22] H. Xuemei, S. Yukun, and B. Bo, Journal of Nanomaterials 2016, 1 (2016); https://doi.org/10.1155/2016/7589028